

8-2014

DEVELOPING A PREDICTIVE MODEL OF HEART WALL MOTION IN FLUOROSCOPIC IMAGES

Christopher Hawkins
Clemson University, hawkin4@clemson.edu

Follow this and additional works at: https://tigerprints.clemson.edu/all_theses

 Part of the [Computer Sciences Commons](#)

Recommended Citation

Hawkins, Christopher, "DEVELOPING A PREDICTIVE MODEL OF HEART WALL MOTION IN FLUOROSCOPIC IMAGES" (2014). *All Theses*. 1908.
https://tigerprints.clemson.edu/all_theses/1908

This Thesis is brought to you for free and open access by the Theses at TigerPrints. It has been accepted for inclusion in All Theses by an authorized administrator of TigerPrints. For more information, please contact kokeefe@clemson.edu.

DEVELOPING A PREDICTIVE MODEL OF HEART WALL MOTION IN
FLUOROSCOPIC IMAGES

A Thesis
Presented to
the Graduate School of
Clemson University

In Partial Fulfillment
of the Requirements for the Degree
Master of Science
Bioengineering

by
Christopher Millard Hawkins
August 2014

Accepted by:
David Kwartowitz, Committee Chair
Delphine Dean
Bruce Gao

ABSTRACT

Image guided surgery (IGS) is an integral part of minimally invasive surgery. IGS combines pre- and perioperative images acquired from different imaging modalities to give the surgeon a more complete view of the internal organs. These modalities include computed tomography, magnetic resonance imaging, and fluoroscopy, to name a few. Fluoroscopy is also known as video x-ray and is becoming increasingly popular in procedures around the heart.

Unfortunately, this increase in fluoroscopy use also brings an increase in exposure to ionizing radiation for the patient and the surgeon. This radiation can lead to increased cancer risk and a number of other problems. Studies show that medical radiation exposure has increased six times from 1992 to 2009. This exposure accounts for approximately half of all radiation exposure that humans receive with background radiation being the only source larger. Of the medical exposure, fluoroscopy accounts for approximately 25%.

An increasingly popular trend in IGS is the use of predictive modeling. Davatzikos, et al, presents a framework for predictive modeling of anatomical structures but focuses on simple structures like ovals and circles. We seek to apply this framework to a more complex organ with more complex motions such as the heart. A predictive model of the heart could provide the surgeon with an effective partial replacement to fluoroscopy. This could significantly reduce radiation exposure as well as the risks of associated diseases.

ACKNOWLEDGMENTS

I would first like to thank my Undergraduate and Graduate advisor, Dr. David Kwartowitz. He encouraged and pushed me to participate in the BS/MS Program offered by the Bioengineering Department at Clemson University. Without his encouragement, I would not have pursued my Master's Degree. I would also like to thank Dr. Kwartowitz and my other committee members, Dr. Delphine Dean and Dr. Bruce Gao, for their support and guidance.

Next, I would like to thank my lab members, Fuad Mefleh, Vipul Pai, and Zahra Ronaghi, for always willing to drop their work to help me with a problem and to participate in my research.

Finally, I would like to thank my mother, wife, and other family members for their unending support throughout my college career. It is because of mother that I have a thirst for knowledge and will never stop learning.

TABLE OF CONTENTS

	Page
TITLE PAGE	i
ABSTRACT.....	ii
ACKNOWLEDGMENTS	iii
LIST OF TABLES	v
LIST OF FIGURES	vi
CHAPTER	
I. INTRODUCTION	1
Overview.....	1
Objectives	3
II. MANUSCRIPT: DEVELOPING A PREDICTIVE MODEL OF HEART WALL MOTION BASED ON FLUOROSCOPY.....	6
Abstract.....	6
Keywords	7
Introduction.....	8
Methods.....	9
Results.....	20
Discussion.....	26
Conclusion	28
III. CONCLUSIONS AND FUTURE WORK.....	30
Conclusions.....	30
Future Work.....	31
REFERENCES	33

LIST OF TABLES

Table		Page
1.	Average Euclidean Distance from Actual to Predicted Boundaries Shown in Figure 9.....	26

LIST OF FIGURES

Figure	Page
1. Sample Frame of Fluoroscopy Video	13
2. Flowchart of Manual Segmentation Process.....	14
3. Fluoroscopy Images of Contracted (a) and Relaxed (b) Hearts with Manually Selected Boundaries (green)	17
4. Fluoroscopy Images of Input of Model (left), s_0 , and Anticipated Output (right) with Manually Selected Boundaries	19
5. Boundaries of Contracted (a) and Relaxed (b) Hearts Manually Segmented by 8 participants.....	21
6. Boundaries of Contracted (red) and Relaxed (green) Hearts Demonstrating Principal Direction of Motion.....	23
7. Comparison of Input to Model (green), s_0 , and Expected Output of Model (red).....	24
8. Comparison of Input to Model (green), s_0 , and Output of Model (red) for Weighting Factor, w , equal to 1	24
9. Comparison of Expected and Actual Output of Model for Weighting Factor, w , of 0.1(a), 0.5(b), 1(c), 2.5(d), 5(e), 10(f).....	25

CHAPTER ONE

INTRODUCTION

Overview

Image guided surgery (IGS) allows surgeons to visualize the patients anatomy during minimally invasive surgery. This is typically done with a combination of pre- and perioperative images from a number of different sources including computed tomography, magnetic resonance imaging, and fluoroscopy, to name a few. The images from these sources are combined to provide more information than would be possible from a single source and greatly enhance the surgeon's ability to accomplish his task. We will focus on the use of fluoroscopy during the operation.

Fluoroscopy

Fluoroscopy is a medical imaging technique used both diagnostically and interventionally. This method uses continuous x-rays, waves of electromagnetic radiation, to show the anatomy of the patient and is often referred to as "video" x-ray. Fluoroscopy may be used for viewing bones, joints, muscles, and organs such as the lungs, kidneys, and heart. This is a popular diagnostic technique because it is non-invasive and may be used to guide minimally invasive diagnostic procedures. More specifically, physicians can locate foreign bodies, view intestinal movements, and even identify blockages of arteries. Interventionally, fluoroscopy is used more as a visual aid. It is useful for placing stents and pacemaker leads as well as visualizing lumbar punctures and biopsy sites [1].

Since the advent of fluoroscopy in the early 1900's, it has been used primarily for diagnosis. However, since the 1980's, this imaging modality has become increasingly popular in interventional procedures. In 1994, an estimated 300,000 coronary angioplasties were performed [2]. The National Cancer Institute has estimated that this number increased to 657,000 procedures in 2002. In addition the number of coronary artery stent procedures doubled over a four-year period starting in 1996 [3]. This large increase in the number of interventional procedures involving fluoroscopy is due to the trend towards minimally invasive procedures. These types of procedures result in substantially reduced risk of infection and shorter hospital stays.

Limitations

In spite of its popularity, the use of fluoroscopy has a couple of problems. The main issue is the exposure of the patient to ionizing radiation, which can result in skin burns and increased incidence of cancer. Another problem is that image quality is partially dependent on the amount of x-ray used to generate the image.

On top of the increase in the number of procedures involving fluoroscopy, the complexity of these procedures has increased resulting in longer surgery times and higher doses of ionizing radiation. According to reports published by the National Council on Radiation Protection and Measurements, the average effective dose of radiation received from medical procedures in the United States increased from 0.53 millisieverts (mSv) in 1992 to 3.00 mSv in 2009. A millisievert is the measure of energy imparted in Joules per weight in kilograms [4]. This exposure accounts for approximately 48% of all radiation

received by the average person [5,6], which is second only to background radiation. Of this medical exposure, interventional and conventional fluoroscopy account for 14% and 11%, respectively [6]. Conventional fluoroscopy is defined as a diagnostic procedure.

A number of techniques are currently employed to reduce radiation exposure. One technique, known as last image hold, allows the surgeon to capture an image of the anatomy and leave it on the screen for consideration. Another technique is dose spreading. This involves adjusting the angle of the beam relative to the patient, which spreads the radiation exposure over a larger area of skin. A third technique involves adjusting the quality of the beam. The intensity of the beam may be lowered which will result in lower quality images. This can affect the surgeon's ability to identify disease or guide tools during interventions. The last technique I will discuss is referred to as pulsed fluoroscopy. This method acquires images at approximately 15 frames per second instead of the typical 30 frames per second [2].

Objectives

The primary object of this study is to apply a framework for predictive modeling to predict heart wall motion in fluoroscopic images. Research shows that this model works well for simple organs and motions, but has not yet been applied to a more complex shape and movement such as that of the heart. This model could potentially be used as a part of IGS systems to reduce patient exposure to ionizing radiation. This would be accomplished by training the model at the beginning of the surgery, then updating it periodically throughout the surgery. The algorithm used to build this model will be

written in MATLAB[®] and will feature the use of principal component analysis (PCA). PCA uses Eigen decomposition to determine the largest directions of variation and then estimate future displacement in this direction.

Significance

As previously mentioned, fluoroscopy is becoming more prevalent as a diagnostic and interventional tool. Along with this increase in prevalence, the procedures are becoming more complex and time consuming. This often results in longer exposure to x-rays, which may have different affects on different patients. The dose of radiation received by a patient actually depends on their size, the examination, as well as the type of equipment and technique used by the surgeon [2]. It is especially important to note that the size of the patient has an affect on dose. This means that children are affected by radiation more than adults due to their size. It is important to reduce radiation exposure, especially in children, without compromising the ability of the surgeon to perform their work.

The development of a predictive model for heart wall motion could provide a reduction in x-ray exposure during interventional fluoroscopy procedures. The model would need a limited number of images to train the algorithm, followed by intermittent imaging to update the model based on real time changes in anatomy. This would be an improvement to current exposure reduction techniques such as intermittent fluoroscopy, last image hold, or pulsed fluoroscopy. These methods do reduced exposure, but result in loss of motion visualization and clarity. A predictive model that can be updated

throughout a procedure would provide constant visualization while maintaining image and video quality.

CHAPTER TWO

MANUSCRIPT: DEVELOPING A PREDICTIVE MODEL OF HEART WALL MOTION BASED ON FLUOROSCOPY

Christopher M. Hawkins, Dr. David M. Kwartowitz

Department of Bioengineering, Clemson University, Clemson, SC

This manuscript will be submitted for publication in Int J CARS.

Abstract

Purpose

Radiation exposure due to medical procedures increased six times between 1992 and 2009 in the United States. One of the largest medical sources is fluoroscopy [5,6]. A predictive model of heart wall motion could be used to reduce this exposure without reducing the surgeon's ability to visualize the anatomy. To accomplish this, we seek to apply Davatzikos's framework for predictive modeling of anatomy to the more complex anatomy of the heart [8].

Methods

Principal component analysis (PCA) determines the main directions of motion in an image and reduces the complexity of the problem. We used Davatzikos's framework to develop a model that predicts heart wall motion based on a new starting point that was not in the training set. We determined the boundary of the heart in multiple training samples using manual segmentation and predicted a new boundary based on a new input

boundary. We measured the average distance between points of the predicted boundary and the expected boundary to determine the accuracy of the model.

Results

The manual segmentation process showed considerable variation between users. However, using three training samples, we were able to predict the deformation of the heart wall. The prediction showed the correct direction of motion and maintained the shape of the heart. The prediction was within 3 mm on average of the anticipated deformation.

Conclusions

We were able to predict the deformation of the heart and believe that this framework would be effective if certain limitations could be reduced. The model is computationally expensive and requires 15 minutes to an hour to run depending on the computer. The manual segmentation process needs to be replaced with an automatic segmentation. Evidence exists to suggest that this method of predicting heart wall motion is possible and should be pursued further.

Keywords

Principal Component Analysis (PCA). Fluoroscopy. Predictive Model. Heart Wall Motion. Eigen Decomposition.

Introduction

Fluoroscopy is becoming an increasingly popular diagnostic and interventional technique in the medical field. Fluoroscopy uses x-rays to obtain a constant video of a patient's body. This gives the doctor the ability to see the change in anatomy over time during minimally invasive procedures. Fluoroscopy is used in barium x-rays, cardiac catheterization, arthrography and many other procedures. The main risk associated with fluoroscopy is exposure to ionizing radiation, which can cause severe skin burns and potentially lead to cancer. These risks increase with the increased use of fluoroscopy. One report shows that as much as 25% of all medical exposure to ionizing radiation is due to fluoroscopy [6].

The dose of radiation delivered to the patient depends on a number of variables including patient size, equipment, and physician technique [2]. Adjusting technique is currently the main way to reduce exposure to radiation during procedures. One technique reduces the acquisition rate of the system so that fewer images are taken per second. Another technique allows the physician to acquire video when needed and holds the last image on the screen when video is not needed. This gives the physician a reference to continue the procedure [2]. These techniques reduce radiation exposure to the patient but are not ideal. They may result in reduced image quality and loss of the ability to see interventional tools in real time.

The limitations and dangers of ionizing radiation in fluoroscopy show that a new solution is necessary. Patients and physicians would benefit from a method of visualizing

the anatomy while reducing exposure to x-rays. We believe the development of a predictive model of the heart wall motion in fluoroscopy would be an acceptable solution.

Predictive modeling using principal component analysis (PCA) is becoming increasingly popular in image processing and image guided surgery. PCA is used in a number of ways including facial recognition, image compression, and modeling motion in systems. The main goal is to reduce the amount of data required to characterize a system or, in the words of Jolliffe, “to reduce the dimensionality of a data set [7].” PCA examines covariance of a system using singular value decomposition or, more specifically, Eigen decomposition. In an image, the eigenvectors describe a certain direction of motion and the corresponding eigenvalue describes the magnitude of the motion in that direction.

Christos Davatzikos wrote about applying principal component analysis to the development of a predictive model of anatomical deformations [8]. This paper seeks to apply Davatzikos’s framework to the development of a predictive model of the heart in fluoroscopy.

Methods

We will first review the theory presented in Davatzikos’s article in IEEE Transactions on Medical Imaging [8]. Then we will discuss the process of using the predictive model in order to predict movement of the heart wall. The program for the model was written using MATLAB® R2014a.

Predictive Model Based on Principal Component Analysis

There are several methods for modeling movement or deformations of structures. When developing a model, it is important to determine the principle modes of variation of shape, deformation, and the principal modes of covariation between these two [8]. This method of modeling anatomical deformations is becoming increasingly popular and important. All of the information presented in this section is a review of Davatzikos's work [8].

The equation for the model involves a number of variables. First, a vector \mathbf{s} contains a collection of points that define the shape of interest. In the case of this research, \mathbf{s} will be an “n” by 2 vector that contains x-y coordinates, which outline a heart in a fluoroscopic image. “n” is the number of coordinates used to mark the boundary A second vector, \mathbf{q} , defines the deformation of \mathbf{s} by describing the change in the x and y directions. Both vectors are reshaped into 1 by 2*n row vectors and then vertically concatenated to form a third vector, \mathbf{x} [8].

$$\mathbf{x} = \begin{bmatrix} \mathbf{s} \\ \mathbf{q} \end{bmatrix} \quad (1)$$

We can assume that \mathbf{x} follows a multivariate Gaussian distribution [8]. The probability density function of \mathbf{x} can be defined by the mean, μ , and the covariance matrix, \mathbf{C} [8].

$$\mu = \begin{bmatrix} \mu_s \\ \mu_q \end{bmatrix} \quad (2)$$

$$C = \begin{bmatrix} C_{ss} & C_{sq} \\ C_{sq} & C_{qq} \end{bmatrix} \quad (3)$$

In equation (3), C_{ss} and C_{qq} represent the variance in \mathbf{s} and \mathbf{q} , respectively. C_{sq} represents the covariance between \mathbf{s} and \mathbf{q} . Equation (2) and (3) can be estimated using a set of training samples. This will be discussed in greater detail in future sections. If we have multiple training sets, then we will have multiple vectors x_i , $i = 1, \dots, K$. Next we obtain the two eigenvectors and eigenvalues for each of the covariance matrices [8].

$$v_i = \begin{bmatrix} v_{s_i} \\ v_{q_i} \end{bmatrix}, i = 1, \dots, K - 1 \quad (4)$$

In equation (4), v_{s_i} and v_{q_i} are the parts of v_i corresponding to \mathbf{s} and \mathbf{q} , respectively. Next, we can combine equations (1), (2), and (4) into a new equation to describe \mathbf{x} [8].

$$x = \mu + \sum_{i=1}^M \alpha_i v_i, M \leq K - 1 \quad (5)$$

In equation (5) we denote that we are taking the M largest eigenvectors instead of the entire set. This causes minimal loss of information and results in a reduction of complexity. The new variable introduced in equation (5), α_i , $i = 1, \dots, M$, completely represents \mathbf{s} and \mathbf{q} as long as the mean and eigenvectors are determined from training samples. Equation (5) can be split in order to calculate \mathbf{s} and \mathbf{q} separately [8].

$$s = \mu_s + \sum_{i=1}^M \alpha_i v_{s_i} \quad (6a)$$

$$q = \mu_q + \sum_{i=1}^M \alpha_i v_{q_i} \quad (6b)$$

Noting that equation (5) can be split into equation (6a) and (6b) will be important when using the model to predict deformations. We can write equation (5) in a general form [8]:

$$x = \mu + Va \tag{7}$$

where \mathbf{a} is a vector containing all α_i , $i = 1, \dots, M$. It is also important to define the probability density function of \mathbf{a} , $g(\mathbf{a})$, as [8]:

$$g(\mathbf{a}) = \exp\left(-\sum_{i=1}^M \frac{\alpha_i^2}{2\lambda_i}\right) \tag{8}$$

where λ_i is the i^{th} eigenvalue.

The equations presented above are the framework for building the model. The next step involves producing the vector \mathbf{x} by finding the points outlining the heart in a number of training samples.

Finding the Heart in Fluoroscopy

One of the limitations of x-ray is the low visibility of soft tissue such as the heart. It is also difficult to differentiate between the heart, arteries, and veins. The surrounding bones and remnants of previous surgeries may further obscure the view of the heart. This is all demonstrated in Figure 1. Due to these difficulties, automatic segmentation of the heart was extremely difficult. Instead, we used manual segmentation.

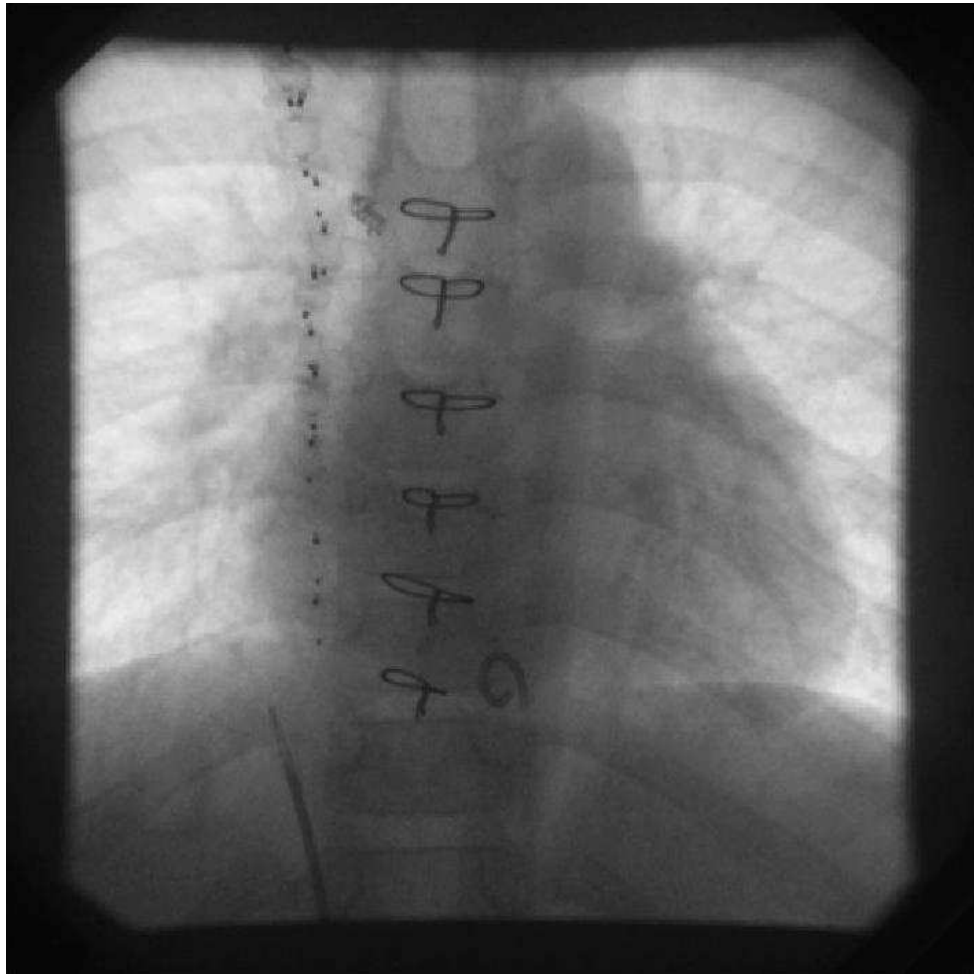


Figure 1: Sample Frame of Fluoroscopy Video

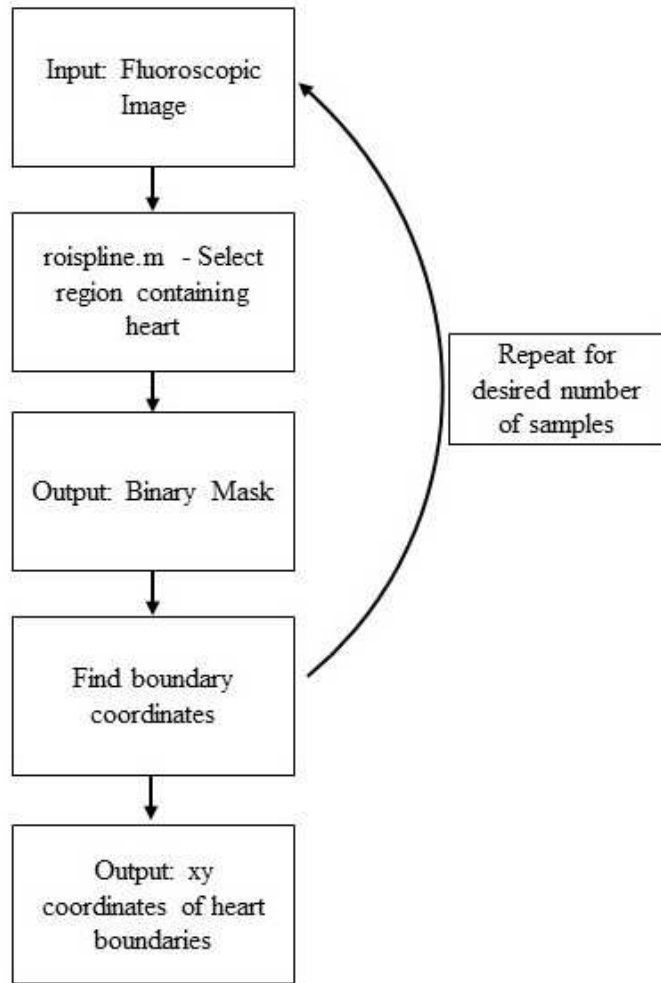


Figure 2: Flowchart of Manual Segmentation Process

The manual segmentation process is outlined in Figure 2. We first picked a frame in which we wanted to determine the boundaries of the heart. This image was used as an input to a program called roispline.m, which was pulled from the MATLAB® Central File Exchange. The program allows the user to select points on the input image and connects those points with splines. This allowed us to select the heart region with fewer points than would have been necessary for other MATLAB® functions. The roispline function output a binary mask where pixels inside the selected region were labeled as true

or “1.” The mask was fed to another MATLAB® function that found the boundary coordinates by locating the edge of the true region of the mask. The output of this function was the x-y coordinates of the boundary of the heart. These coordinates were stored as a variable for further processing. This process was repeated for the number of samples desired for training the model. In this study we used three samples, which required manual segmentation of 6 images.

After finding all of the boundaries, we had to adjust the number of coordinates that describe each boundary. For the model, all vectors \mathbf{s} and \mathbf{q} had to be the same size. In order to accomplish this, we found the boundary set that had the fewest number of points. Then we reduced the other boundary sets to the size of the smallest set. For our data, all boundary sets were reduced to 700 points.

Training The Model

In order to train the model, we used three samples. This involved finding three frames where the heart was contracted and three frames when the heart was relaxed. We ran the Manual Segmentation Process discussed in the previous section on each of the six frames. In order to eliminate bias, we had eight participants from the lab manually segment the heart in ten frames randomly selected from the six used for training the model and two frames for using the model. Each participant was shown an image with the heart and rib cage. They were also told that the base of the heart is typically located between the second and third ribs with the apex between the fifth and sixth ribs. The results were gathered by frame and averaged together using a nearest neighbor algorithm.

Figure 3 shows each frame as well as the outline of the heart from the averaging process. The x-y coordinates for the boundaries in Figure 3a were averaged together using a nearest neighbor algorithm to form vector \mathbf{s} . The x-y coordinates for the boundaries in Figure 3b were subtracted from the coordinates in Figure 3a to get displacement vectors. These three vectors were averaged together to get vector \mathbf{q} .



Figure 3: Fluoroscopy Images of Contracted (a) and Relaxed (b) Hearts with Manually Selected Boundaries (green)

The next step in the process was to calculate the covariance matrix of each vector \mathbf{x} . This resulted in three covariance matrices, which generated six eigenvalues and six eigenvectors. Next we determined an average vector \mathbf{x} for calculation purposes and the mean, \mathbf{u} , from equation (2). Then we sorted the eigenvectors by the magnitude of their eigenvalues and kept the top 90% of eigenvalues. The associated eigenvectors were used to make vector \mathbf{V} in equation (7). The final step in training the model was to solve equation (7) for vector \mathbf{a} . As previously mentioned, this vector completely characterizes the samples acquired so far and can be used as a starting point to predict future deformations. Once we calculated \mathbf{a} , we proceeded to the next step of predicting deformation based on a new starting point.

Using the Model

In order to use the model, we first picked a new starting frame for which we wanted to predict the deformation and used the procedure from Figure 2 to determine the boundaries. As previously mentioned, we had participants from the lab pick boundaries for the relaxed and contracted heart. The images of the frames and selected boundaries are shown in Figure 4. The boundaries of the contracted heart in Figure 4 were used as a new vector \mathbf{s}_0 . The boundaries of the relaxed heart in Figure 4 were used to determine the accuracy of the model.

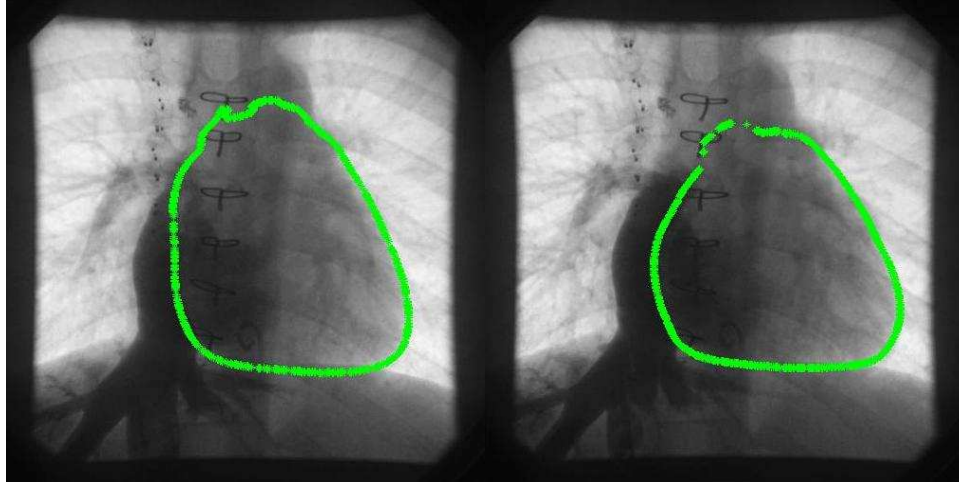


Figure 4: Fluoroscopy Images of Input of Model (left), s_0 , and Anticipated Output (right) with Manually Selected Boundaries

Next, we used the Levenberg-Marquardt nonlinear optimization scheme in order to minimize the following objective function [8]:

$$\mathcal{E}(a) = \|s - s_0\|^2 + w \frac{1}{g(a)} \quad (9)$$

where vector \mathbf{s} refers to the original \mathbf{s} from the training samples, \mathbf{s}_0 is the new starting point, w is a relative weighting factor and $g(a)$ is the probability density function shown in equation (8). The first half of the equation favors a vector \mathbf{a} that gives an output close to the initial starting point, while the second half of the equation favors a PDF similar to the original vector \mathbf{a} . This equation is expanded below:

$$\mathcal{E}(a) = \left\| \mu_s + \sum_{i=1}^M \alpha_i v_{s_i} - s_0 \right\|^2 + w \frac{1}{g(a)} \quad (10)$$

We utilized this equation by running the optimization scheme with equation (10) and vector \mathbf{a} as a starting point. The output of the optimization scheme was a new vector $\hat{\mathbf{a}}$,

which, along with equation (6b), was used to calculate an estimate of deformation, vector $\hat{\mathbf{q}}$. This is shown in equation (11), where μ_q and v_{qi} were calculated in the training set.

$$\hat{q} = \mu_q + \sum_{i=1}^M \hat{\alpha}_i v_{qi} \quad (11)$$

It is important to note that the process of determining $\hat{\mathbf{a}}$ was the most computationally expensive step in this process. With this information, we calculated the estimated boundary of the relaxed heart shown in Figure 4 and compared the two boundaries to determine the accuracy of the model.

Results

As previously mentioned, the heart is difficult to find in fluoroscopy. The purpose of randomly sampling lab members' manual segmentation of the heart was twofold. First, we wanted to eliminate bias for purposes of showing the model worked properly. Second, we wanted to show the variability between users during the manual segmentation process. This variability is shown in Figure 5. The images in this figure correspond to those in Figure 3. Figure 3 shows the averages of the boundaries in the images of Figure 5.

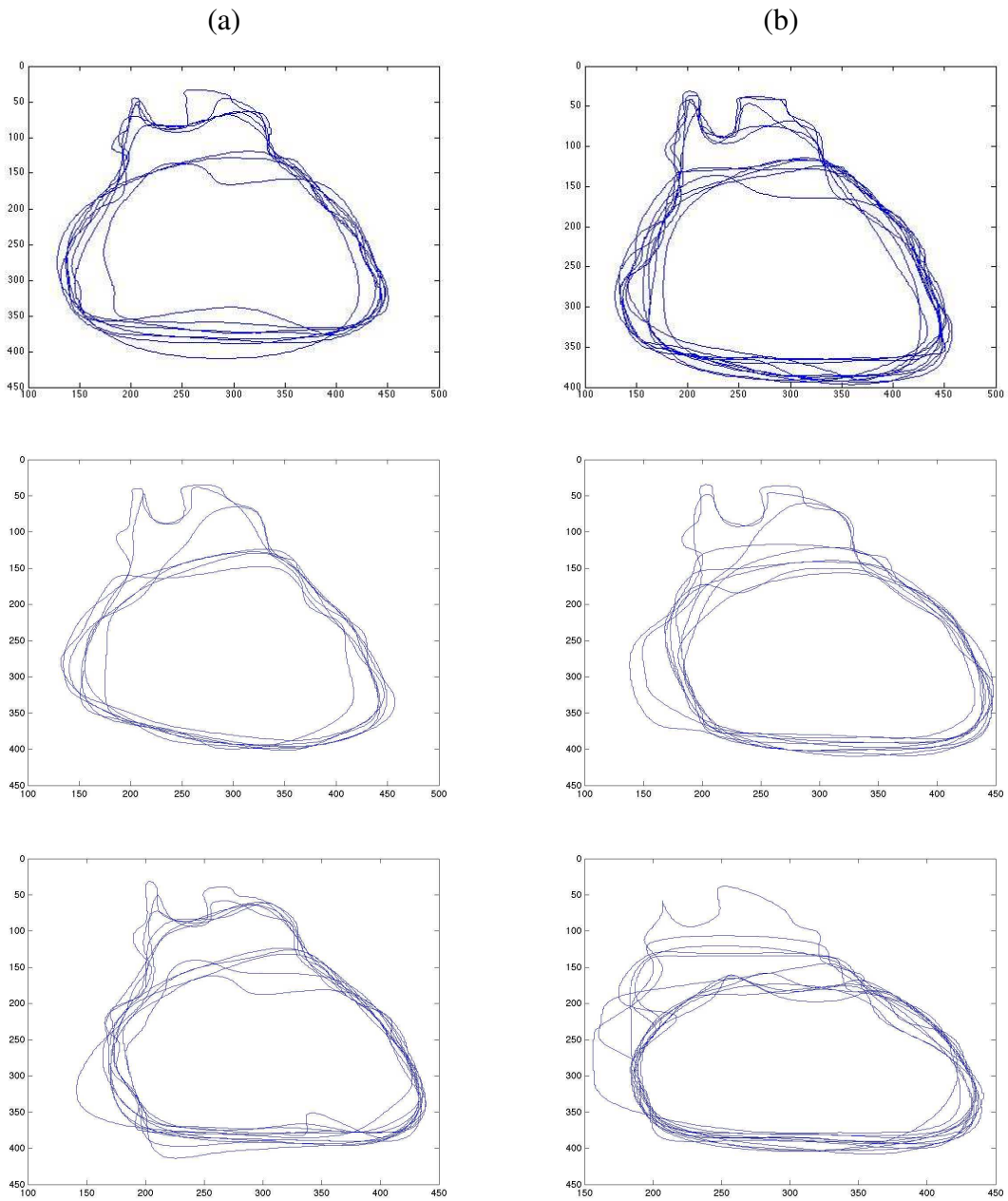


Figure 5: Boundaries of Contracted (a) and Relaxed (b) Hearts
Manually Segmented by 8 participants

It is important to determine the main direction of motion of the heart in order to show the model is working properly. By looking at the fluoroscopy video, as well as the boundaries of the relaxed and contracted heart together, we can see the direction with the largest variation. The boundaries of the relaxed heart are overlaid with the boundaries of the contracted heart to show this direction of variation in Figure 6 for the three training samples from Figure 3.

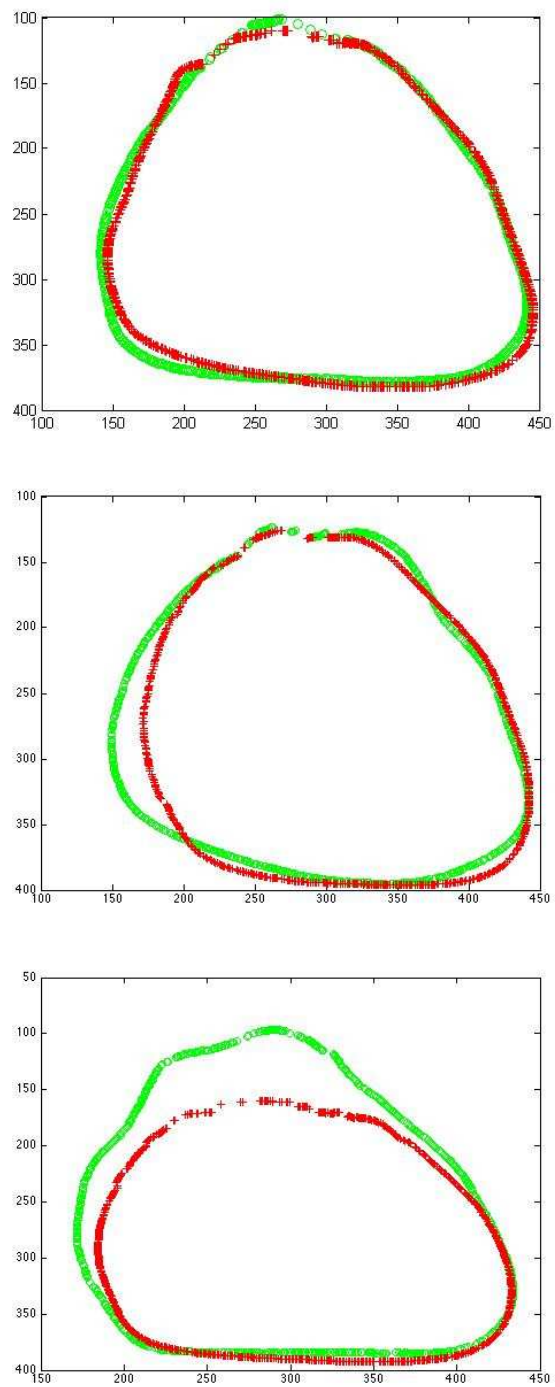


Figure 6: Boundaries of Contracted (red) and Relaxed (green) Hearts Demonstrating Principal Direction of Motion

Figure 7 shows the boundaries of the relaxed heart used as s_0 for the input of the model as well as the expected result of the contracted heart. Figure 8 shows the input to the model, s_0 , along with the predicted relaxed heart. Figure 9 shows the expected output of the model along with the actual output of the model when the weighting factor w of the objective function, Equation (9), is set to values ranging from 0.1 to 10.

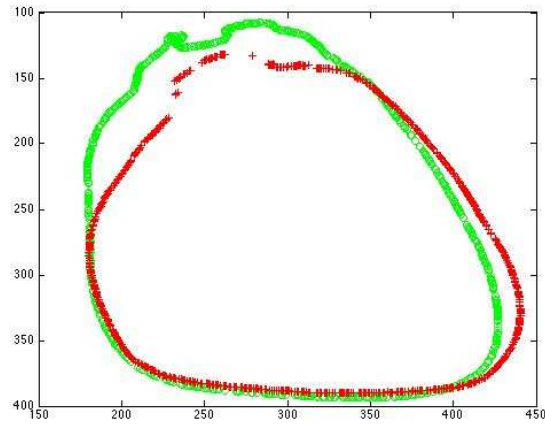


Figure 7: Comparison of Input to Model (green), s_0 , and Expected Output of Model (red)

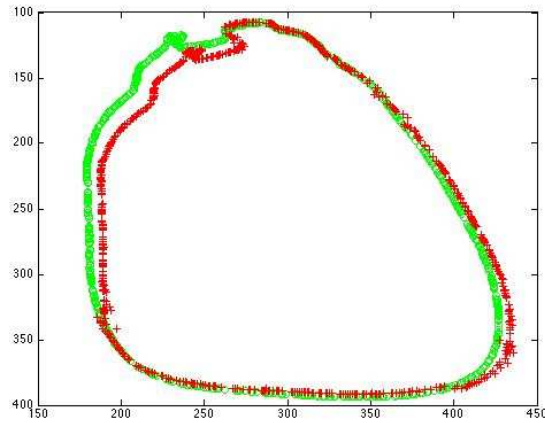


Figure 8: Comparison of Input to Model (green), s_0 , and Output of Model (red) for Weighting Factor, w , equal to 1

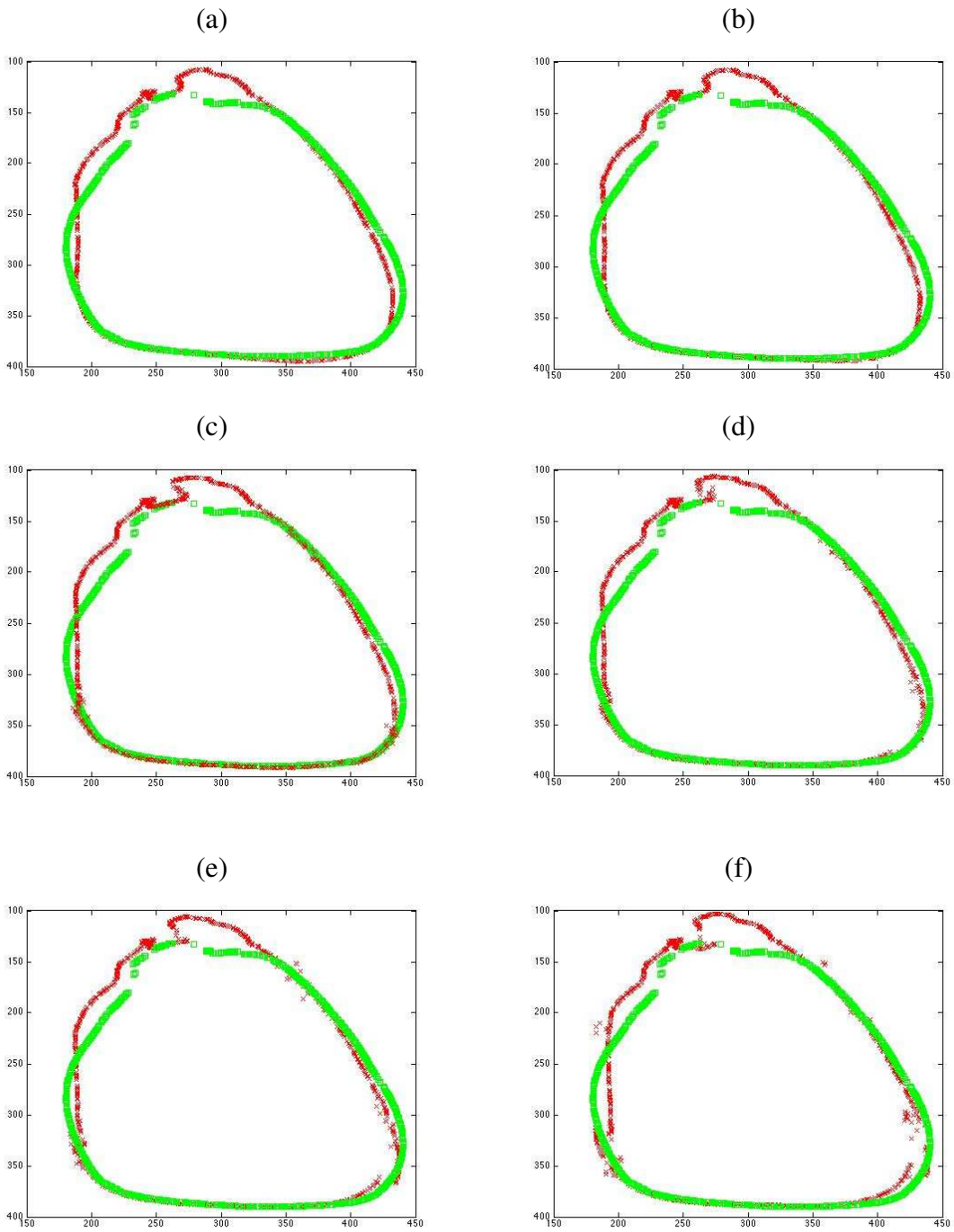


Figure 9: Comparison of Expected and Actual Output of Model for Weighting Factor, w , of 0.1(a), 0.5(b), 1(c), 2.5(d), 5(e), 10(f)

The values in Table 1 give a general idea of the accuracy of the model for varying weighting factors, w . The distance listed for each w is the average Euclidean distance between pixels of the expected and actual outputs of the model. The Euclidean distance was calculated between nearest neighbor pixels. We then calculated the size of the pixels based on the dimensions of the image intensifier and the number of pixels that span the image. This gives the average distance in millimeters (mm).

Table 1: Average Euclidean Distance from Actual to Predicted Boundaries Shown in Figure 9

w	0.1	0.5	1	2.5	5	10
Distance (mm)	3.01	2.98	3.00	3.00	3.08	3.35
Standard Deviation (mm)	2.56	2.63	2.66	2.71	2.70	2.93

Discussion

The images in Figure 6 show the variability between users of the manual segmentation process. The participants in the manual segmentation process were all untrained students. Each one was briefly told how to locate the heart using the ribs and shown a reference image of the heart in the rib cage. The variance in boundary location is most likely due to the perception of the participant as well as the blurred boundary of the heart in the image. The variability in the selected boundaries demonstrates the need for a better segmentation process. Ideally, this process would be automatic in order to eliminate human biases and error. Unfortunately, at this time, segmentation algorithms

are not able to effectively segment the heart. This is due to the poor ability of fluoroscopy to differentiate between soft tissues.

By looking at the images in Figure 6 and having an understanding of the anatomy of the heart, we can determine the expected principal direction of variation. In the images of Figure 6, this direction of variation is diagonally from the upper left hand corner to the bottom right hand corner. In anatomical terms, the main direction of variation is from the apex of the heart to the right side of the base of the heart. This direction of motion is a result of the contraction of the left ventricle.

The series of figures from 7 to 9 are the most important to this paper. Figure 7 shows the input to the model and the expected output together, confirming the expected principal direction of motion. Figure 8 shows the input to the model and the actual output of the model for weighting factor, w , equal to 1. From this image we can clearly tell that the model does capture the principal direction of motion determined by the training samples. The next step is to determine the accuracy of the model.

The images of Figure 9 demonstrate an attempt to adjust the weighting factor, w , of the objective function, Equation (9), in order to obtain a better prediction of the deformation. It is apparent that a w of greater than 1 causes the model to work improperly. The output shows non-uniform boundaries with increasingly inaccurate outputs as w increases. This is further confirmed by the values in Table 1. As w increases from 1, so does the average distance. This indicates that the individual points of the actual and predicted boundaries are getting further apart on average. The standard

deviation also increases indicating that the model has reduced accuracy and precision with increasing w .

When we look at values of w between 0 and 1, it appears that 0.5 yields the best results. This is demonstrated primarily by the values in Table 1, which indicate that the average distance between boundary points is the lowest at 2.98 mm. The values of Table 1 do not provide definitive proof that any w is better than the other. The range of distances is less than 0.5 mm, demonstrating that w does not greatly affect the accuracy of the model. Other aspects of the model may need to be adjusted to increase accuracy. It is interesting to note that at w equal to 0.1, the average distance increases to levels similar to w equal to 1. However, the standard deviation continues to decrease with decreasing w . This indicates that decreasing w increases precision and accuracy up to a point. Further testing would be required to better characterize the effect of w on this data set as well as the variation in effect on different data sets.

Conclusion

Examination of Davatzikos's framework for a predictive model demonstrates that it could be applied to a complex organ such as the heart. The simple model developed here does maintain the shape of the heart in the output and captures the principal direction of variation. These are two important aspects of the model. Because we are dealing with medical images and surgical guidance, accuracy is the most important aspect of the model. Our data shows that at the model's best, it will produce a prediction within 3 mm of the expected boundary. Other aspects of the model should be tested to try to

increase accuracy. There are currently a number of limitations to this method including the image acquisition method itself and the lack of ability to automatically segment the heart. I believe that, if the effects of these two limitations could be minimized, this model would be effective at predicting the heart wall motion. The next challenge is to reduce computation time, which ranged from 15 to 60 minutes during this study.

CHAPTER THREE

CONCLUSIONS AND FUTURE WORK

Conclusions

The framework for predictive modeling of anatomical structures presented by Davatzikos was evaluated for use with the more complex anatomy of the heart [8]. For this study we developed a program in MATLAB® using Davatzikos's framework. A manual segmentation process was used to find the boundaries of the heart in fluoroscopy images and these boundaries were used to train the model as well as test the accuracy.

The manual segmentation process showed a large amount of variability between users of this process. This is due to a number of problems. First, the participants of this part of the study were untrained in finding the heart in fluoroscopy. Second, fluoroscopy does not differentiate between soft tissues. This results in blurred lines at boundaries.

In spite of the limitations of the manual segmentation process, the model maintains the shape of the heart as expected and captures the main direction of motion due to the contraction of the left ventricle. The data shows that the model is within approximately 3 mm of the anticipated output.

The model is computationally expensive. During testing, we experienced computation times ranging from 15 minutes to an hour depending on the computer used. This is due to a number of issues including the slow speed of the MATLAB® programming language and the size of matrices required to run the optimization scheme. Despite the limitations of the study, the model appears to effectively predict the heart wall motion.

Future Work

There are a number of major steps that could be taken to improve this model. The most important would be to develop an algorithm for automatically or semi-automatically segmenting the heart. These would eliminate bias and other errors associated with manual segmentation of the heart. It would also make the model more practical for clinical use because it would eliminate or reduce the hands on time required by the surgeon or assistant to segment the heart manually. Ultimately, a fully automatic algorithm would be best.

The next step would be to assess the accuracy of the model to determine acceptable limits of distance between expected and actual model outputs. Because this model could potentially be used for navigating during minimally invasive surgery, it is extremely important to minimize this error as much as possible. Other aspects of the model should be tested to determine the effect on accuracy including the number of samples for training, weighting factors within the PDF of vector \mathbf{a} , and potentially using the entire image of the heart instead of just the boundaries.

Another area requiring extra work is reducing computation time. Even at our best time of approximately 15 minutes, this model could not be used during a surgery. In a real setting, by the time this prediction is made it would be useless information because the deformation would have already occurred. The prediction section of this model would need to be performed multiple times throughout the surgery in order to constantly update the view for the surgeon. The computation would need to occur in a matter of

microseconds in order for the model to be practical for use in the operating room. In order to reduce these times, the algorithm could be written a fast programming language. The algorithm could also be programed to use few eigenvectors.

The final area of future work is integration into an IGS system. Work is being performed to track surgical tools using electromagnetics (EM). If these two technologies could be combined, surgeons would have the ability to visualize the heart as though it were being imaged in real time and see the EM tracked tool in these images. Ultimately, this would help reduce the patient and surgeon's exposure to the ionizing radiation of fluoroscopy.

References

- [1] "Fluoroscopy Procedure." *Health Library*. Johns Hopkins Medicine. Web2014.
- [2] Mahesh, M. "Fluoroscopy: Patient Radiation Exposure Issues." *Radiographics* 21.4 (2001): 1033-45. Print.
- [3] Institute, National Cancer. "Interventional Fluoroscopy □Reducing Radiation Risks for Patients and Staff " *NIH Publication No. 05-52862005*. Print.
- [4] Measures, International Bureau of Weights and. "The International System of Units (Si)." 8th ed2006. Print.
- [5] Thurston, Jim. "Book Review: Ncrp Report No. 160: Ionizing Radiation Exposure of the Population of the United States." *PHYSICS IN MEDICINE AND BIOLOGY* 55 (2010): 1. Print.
- [6] *Ionizing Radiation Exposure of the Population of the United States: (Report No. 160)*: National Council on Radiation Protection and Measurements (NCRP), 2009. Print.
- [7] Jolliffe, I.T. "Principal Component Analysis." *Springer Series in Statistics*. 2nd ed: Springer, 2002. 489. Print.
- [8] Davatzikos, C., et al. "A Framework for Predictive Modeling of Anatomical Deformations." *IEEE Trans Med Imaging* 20.8 (2001): 836-43. Print.